Pattern formation, synchronization, and outbreak of biodiversity in cyclically competing games

Wen-Xu Wang,[1] Xuan Ni,[2] Ying-Cheng Lai,[1,2,3] and Celso Grebogi[3]

[1]*School of Electrical, Computer, and Energy Engineering, Arizona State University, Tempe, Arizona 85287, USA*

[2]*Department of Physics, Arizona State University, Tempe, Arizona 85287, USA*

[3]*Institute for Complex Systems and Mathematical Biology, King's College, University of Aberdeen, Aberdeen AB24 3UE, United Kingdom*

(Received 24 July 2010; revised manuscript received 16 November 2010; published 27 January 2011)

Species in nature are typically mobile over diverse distance scales, examples of which range from bacteria run to long-distance animal migrations. These behaviors can have a significant impact on biodiversity. Addressing the role of migration in biodiversity microscopically is fundamental but remains a challenging problem in interdisciplinary science. We incorporate both intra- and inter-patch migrations in stochastic games of cyclic competitions and find that the interplay between the migrations at the local and global scales can lead to robust species coexistence characterized dynamically by the occurrence of remarkable target-wave patterns in the absence of any external control. The waves can emerge from either mixed populations or isolated species in different patches, regardless of the size and the location of the migration target. We also find that, even in a single-species system, target waves can arise from rare mutations, leading to an outbreak of biodiversity. A surprising phenomenon is that target waves in different patches can exhibit synchronization and time-delayed synchronization, where the latter potentially enables the prediction of future evolutionary dynamics. We provide a physical theory based on the spatiotemporal organization of the target waves to explain the synchronization phenomena. We also investigate the basins of coexistence and extinction to establish the robustness of biodiversity through migrations. Our results are relevant to issues of general and broader interest such as pattern formation, control in excitable systems, and the origin of order arising from self-organization in social and natural systems.

DOI: 10.1103/PhysRevE.83.011917 PACS number(s): 87.23.Cc, 02.50.Ey

I. INTRODUCTION

Biodiversity is ubiquitous in nature and fundamental to evolution in ecosystems [1–3]. However, a significant challenge remains in understanding biodiversity since, by the principle of natural selection, only fitter species are supposed to be capable of surviving from interactions and competitions with other species for limited resources. To resolve this dilemma, evolutionary game theory [4–8] has been used as a paradigm to address the coexistence of competing species, which is the key to sustaining biodiversity.

A fundamental type of interactions in ecosystems is cyclic, nonhierarchical competitions. They have been observed in a plethora of real ecosystems ranging from microbes to mating strategies of side-blotched lizards in California [9–12]. A paradigmatic system to study the role of competitions in biodiversity is the classical, cyclic game of rock-paper-scissors. One approach is *macroscopic* in the sense that the mathematical models are aimed at describing the evolution of the populations of competing species, which are assumed to be well mixed. In this macroscopic approach, any species is treated as a whole through its population [13–16]. An interesting result from this approach is that cyclic competitions alone are not sufficient to support species coexistence [14,17]. The ubiquity of the coexistence phenomenon in nature suggests that additional factors must exist to promote coexistence and consequently, biodiversity. To identify these additional factors and also to capture the complex interacting dynamics among individuals of competing species, *microscopic* game models incorporating stochastic interactions on spatially extended scales have been exploited with the remarkable result that, due to stochasticity and local interactions, coexistence can arise even in the presence of species dispersal [12]. Since then, the role of mobility in coexistence in microscopic game models has been investigated [18–21], where it was found that strong *local* mobility can cause nonlocal interactions, which under certain circumstances tend to hamper coexistence through the formation of moving spiral waves of population densities in the physical space [20]. The roles of epidemic spreading [22] and intra-species competition [23] in species coexistence have also been studied. A seemingly accepted notion in the field is, then, that strong mobility is detrimental to biodiversity.

In this paper, we report a phenomenon that is in sharp contrast to the existing notion: species migration across vast spatial scales can in fact promote coexistence. Such movements are indeed common in ecosystems [24]. Since long-distance migrations can be regarded effectively as an extremely strong type of mobility, according to the conventional wisdom, coexistence would be disfavored or even prohibited. However, our studies have revealed, strikingly, that migration favors coexistence and thereby promotes biodiversity.

To be concrete, we consider species movements on two distinct spatial scales (intra-patch and inter-patch migration), and study stochastic games microscopically by focusing on the formation and the dynamics of self-organized patterns of species densities. As will be explained, our microscopic model of inter-patch migration based on stochastic interactions is quite different from the coupled patchy models described by deterministic differential equations [25–30]. We will show that the combination of intra- and inter-patch migrations can result in a robust type of coexistence characterized by the formation of a surprising class of *target* wave patterns that were found previously but in different contexts such as excitable systems [31–35]. We find that, associated with coexistence, synchronization and time-lagged synchronization among spatial patterns in different patches emerge, implying the persistence of coexistence. An appealing feature of time-lagged synchronization is that it can potentially be used

to predict the spatiotemporal evolution of species. We also find that the interplay between the two types of migration can result in a spontaneous outbreak of biodiversity in a world of single species with rare mutations. We establish the robustness of the biodiversity-sustaining target waves with the aid of a basic concept in nonlinear dynamics: basins of attraction in the phase space. All the results will be demonstrated using systematic simulations of microscopic game dynamics and substantiated by theoretical analysis based on nonlinear partial differential equations. Our results not only provide insights into the dynamics of global oscillations induced by long-distance interactions among cyclically competing species [36], but also have implications to the emergence and maintenance of order from randomness and disorder in natural and social systems through self-organization in the absence of any central control.

In Sec. II, we describe the spatial RPS model with both intra- and inter-patch migrations. In Sec. III, we present results on synchronization and lag synchronization among target waves in different patches and introduce an order parameter to quantify the synchronization behaviors. In Sec. IV, we provide analytical results for the observed phenomenon of pattern synchronization. In Sec. V, we present the results of outbreak of biodiversity through rare and random mutations and explore the coexistence of target and spiral waves. In Sec. VI, we investigate attraction basins of coexistence and extinction in the phase space. Conclusions and discussions are presented in Sec. VII.

II. MODEL

We consider multiple-patch systems of three subpopulations (referred to as a, b, and c) under both intra- and interpatch migrations. Within each patch, a, b, and c interact with each other according to the following rules:

$$ab \xrightarrow{u} a\emptyset, \quad bc \xrightarrow{u} b\emptyset, \quad ca \xrightarrow{u} c\emptyset, \tag{1}$$

$$a\emptyset \xrightarrow{\sigma} aa, \quad b\emptyset \xrightarrow{\sigma} bb, \quad c\emptyset \xrightarrow{\sigma} cc, \tag{2}$$

$$a\odot \xrightarrow{\varepsilon} \odot a, \quad b\odot \xrightarrow{\varepsilon} \odot b, \quad c\odot \xrightarrow{\varepsilon} \odot c, \tag{3}$$

where $\emptyset$ represents empty sites and $\odot$ represents any species or empty sites. Relations (1)–(3) define competition, reproduction, and intra-patch migration that occur at the rates u, σ, and ε, respectively. The occurrence probabilities are normalized by $(u+\sigma+\varepsilon)$. Since our focus is on the role of mobility, we set $u=\sigma=1$without loss of generality. The individual mobility is defined as $M=\varepsilon(2N)^{-1}$, which is proportional to the number of sites explored by one individual per time step [20]. Initially, individuals are randomly located over all patches, each of which is represented by a lattice of $L\times L$ sites with open boundary conditions. At each simulation step, a random pair of neighboring sites is selected for one type of interaction from Eqs. (1)–(3) according to its probability. Whether the chosen interaction can actually occur is determined by the states of both sites. An actual time step t is defined when each individual has experienced interaction once on average, i.e., in one time step N pairwise interactions will have occurred.

Inter-patch migration is a type of long-distance species movement among different patches. In a certain period, a mutual migration takes place among patches, where one randomly selected individual migrates from one patch to a random location in the target region of another patch and vice versa (see Fig. 1). To be as general as possible, we assume that the target region can be either a single site or an area. The speed of inter-patch migration is determined by the parameter T_m, the actual time between two successive mutual migrations. Statistically, for $T_m=1$, there are on average N intrapatch interactions. The mobility M and the inter-patch migration time T_m thus constitute two key parameters in the spatial game dynamics. In addition to addressing the role of these two parameters, we will consider the effects of multiple patches and of the position and area of the target region on coexistence.

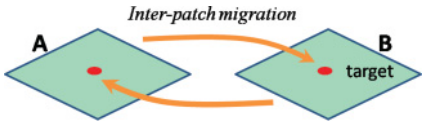

FIG. 1. (Color online) Illustration of interpatch migration in a two-patch ecosystem with open boundary conditions. There is a periodic migration between two patches: at each time step nT_m ($n=1,2,\ldots$), one randomly selected individual migrates from patch A to patch B and vice versa. The migration (target) region can be of any size and at any location in the patch. If the target area contains several sites, we randomly pick one site. If there are more than two patches, each migration individual first randomly chooses a patch and then occupies a target site, regardless of the original individual at the site. The individual with inter-patch migration leaves its site empty in the original patch.

III. PATTERN FORMATION AND SYNCHRONIZATION

A. Synchronization of target waves among patches

We first study an ecosystem of two patches, where a single target region is located at the center of each patch for inter-patch migration. Without the migration, in each patch two species will become extinct and only one species can prevail. When inter-patch migration occurs, a predominant species can arise due to the difference in the initial densities at $t\approx 2500$, as shown in Fig. 2. After this event, species superior to the dominant one in the cyclic-competition loop

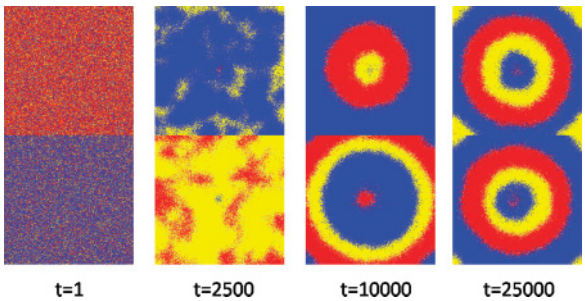

FIG. 2. (Color online) Emergence of target waves and pattern synchronization in a two-patch system with initially mixed populations for $M=0.7\times10^{-4}$ and $T_m=1$. Each patch has size 300×300 and the target is at the center. The initial densities of species in the first patch are $\rho_a=0.6$ and $\rho_b=\rho_c=0.2$, and in the second patch are $\rho_b=0.6$ and $\rho_a=\rho_c=0.2$. Red (gray), blue (dark gray) and yellow (light gray) colors represent the three species a, b, and c, respectively, and empty sites are denoted by gray.

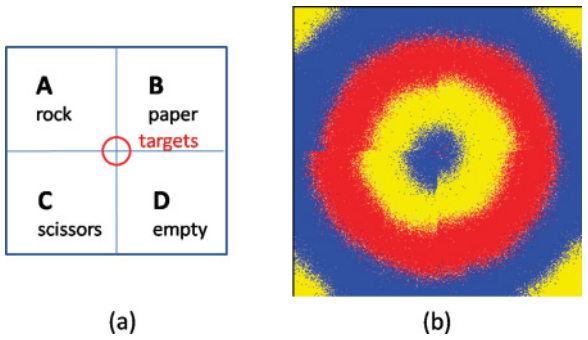

FIG. 3. (Color online) (a) Initial configuration of a four-patch system with noncentral target and (b) synchronization of target waves. The lattice sizes of each single patch is 200×200. The parameters are $M = 3.2 \times 10^{-4}$ and $T_m = 6$. Initially, three species a, b, and c populate patches A, B, and C, respectively, and the fourth patch is empty. To visualize the possible synchronization behavior, the target is set at the corner of each patch and the target corners of the four patches are put together. The boundaries among the four patches are, in fact, disconnected. Target waves are formed in each patch, but as a quarter of a circle, in contrast to the case of central migration targets. The target waves among different patches can still synchronize with identical ring numbers.

appear around the target points in both patches, inducing target waves that emanate from their respective target points and propagate outward. The target waves from the two patches tend to synchronize with each other for $t \gtrsim 25\,000$. When synchronization occurs, it can be maintained and there is then a strong order in the system dynamics. We have examined a three-patch system, where initially there is a single species in each patch and a four-patch system where the target locations deviate from the centers of patches, e.g., at the corner of each patch (see Fig. 3). We observe synchronized target waves as well.

The target area in each patch can have a significant influence on pattern formation and synchronization. As shown in Fig. 4, we observe synchronization of target waves when the target area is small. In this case, time series of the densities of a particular species in the three patches exhibit a phase-synchronized behavior. For a large target area, a strikingly different type of synchronization occurs: time-delayed synchronization. In this case, the time series exhibit the same period T but there is a time lag of about T/N_p among them, where N_p is the number of patches [Figs. 4(b)–4(d)].

B. Order parameter and phase diagram

We introduce an order parameter defined by the phase difference between the species densities. Specifically, the average period can be computed by the time interval between two neighboring peaks. Since the densities in the three patches exhibit similar oscillatory behaviors, we can define an average period $\langle T \rangle$ obtained from, say, ρ_a in three patches. We can then calculate the order parameter of phase synchronization between each pair of patches. For example, for B and C, the order parameter η_{BC} is

$$\eta_{BC} = 1 - \frac{\langle \min(\Delta t_{BC}, \langle T \rangle - \Delta t_{BC}) \rangle_{BC}}{\langle T \rangle / 2}, \qquad (4)$$

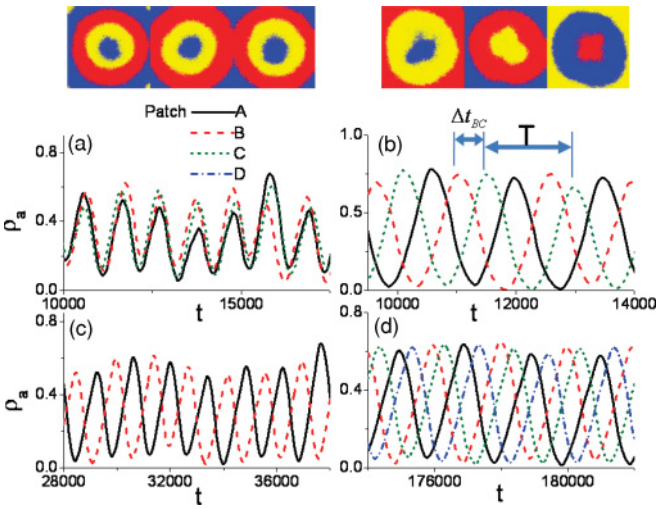

FIG. 4. (Color online) (a) Phase synchronization and (b) time-delayed synchronization among target-wave patterns in a three-patch system for small and large migration-target areas, respectively. The parameters are $M = 0.8 \times 10^{-4}$ and $T_m = 1$. (c) Time-delayed synchronization for a two-patch ($M = 0.6 \times 10^{-4}$) and (d) a four-patch ($M = 1.2 \times 10^{-4}$ and $T_m = 1$) system, where the evolutions of densities of species whose distances from the central target site are less than $L/2$ are displayed. The target radii for synchronization and lag synchronization are 15 and 40, respectively, and $L = 300$.

where $\langle \cdots \rangle_{BC}$ stands for the average over all pairs of neighboring peaks in B and C and Δt_{BC} is the time difference between a peak in B and the closest peak in C, so that the value of $\min(\Delta t_{BC}, \langle T \rangle - \Delta t_{BC})$ is less than $\langle T \rangle/2$. If ρ_a's from B and C display a phase coherence, Δt_{BC} tends to zero and η_{BC}approaches unity. If the phases are incoherent, η_{BC} tends to zero. The overall order parameter η can be defined by the average of order parameters from all patches:

$$\eta = \frac{\eta_{AB} + \eta_{AC} + \eta_{BC}}{3}. \qquad (5)$$

Lag synchronization, however, needs to be characterized by all pairs of order parameters. Since the time delay for each pair is $T/3$, for lag synchronization we have $\eta_{AB} = \eta_{AC} = \eta_{BC} = 1/3$.

The order parameter enables us to quantify the dependence of pattern synchronization on both M and T_m. As shown in Fig. 5, for $M < 2 \times 10^{-5}$, target waves become unstable and break into small spiral waves (the three insets in region I). Once spiral waves have appeared, they are robust, making the appearance of target waves difficult. For large values of T_m, because of the low inter-patch migration frequency, species coexistence in each patch is ruled out. Based on these results, we have identified three regions in the parameter space: (I) spiral-wave region, (II) target-wave region, and (III) extinction region. Of interest is region II, where synchronization occurs as a result of both intra- and inter-patch migration.

C. Transition between synchronization and lag synchronization

We have observed numerically that, as the area of the migration target region is increased, there is a transition from pattern synchronization to lag synchronization, with the latter meaningfully defined by the order parameters calculated from

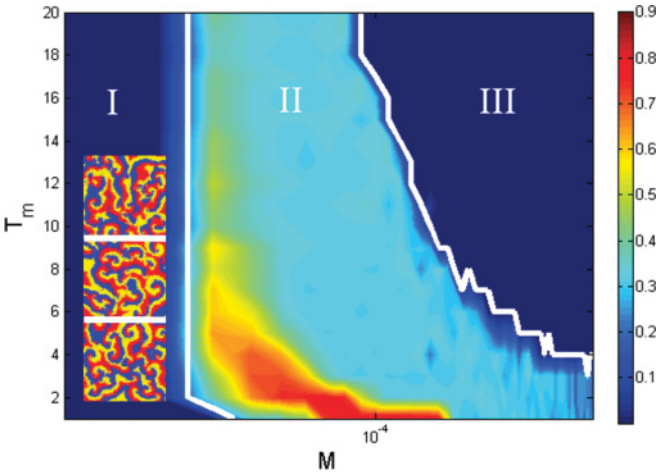

FIG. 5. (Color online) In a three-patch system, dependence of the order parameter η on M and T_m. The radius of migration target is 10, centered at the lattice. Three phases are identified in the parameter space: (I) spiral waves, (II) target-wave region in which there is a synchronization subregion, and (III) extinction region defined by the criterion that in any patch at any time, the number of individuals in a species is less than three. The size of each patch is 300×300 and initially there is a single species in each patch.

all distinct pairs of patch combinations. To distinguish the two types of synchronization from disorder states computationally, we calculate the mean values of all the order parameters and their variances, which can be justified, as follows. When synchronization occurs, all order parameters obtained from different realizations should approach unity and their variances are small. However, for lag synchronization, the values of all order parameters are $1/3$ with small variances as well. For a disorder state, either the mean values are low or the variances are large. Note that order parameters obtained from different realizations should be treated on equal footing.

Figure 6(a) demonstrates the transition from pattern synchronization to lag synchronization as the area of target region is increased. We see that, when the target is a single site, synchronization occurs, where the order parameters have high

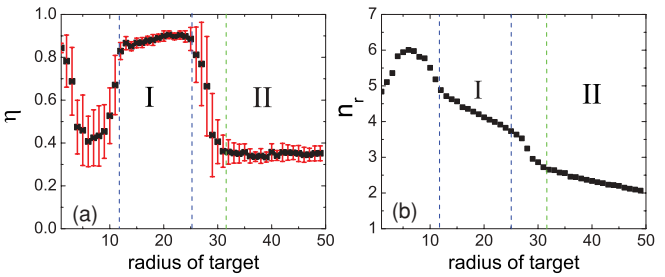

FIG. 6. (Color online) For a three-patch (A,B,C) system, (a) mean value and standard deviation of the order parameter η, and (b) the number of rings n_r as a function of the radius of the target region. Parameters are $L = 300$, $M = 0.8 \times 10^{-4}$, and $T_m = 1$. Data points are obtained from 20 independent realizations, where $\eta = (\eta_{AB} + \eta_{AC} + \eta_{BC})/3$ and the bars represent the standard deviations. There are three distinct dynamical behaviors: synchronization in region I, lag synchronization in region II, and disorder in other regions.

mean values and low variances. As the radius of the target area is increased, the target-wave patterns in all patches degrade and disorder appears, as reflected by the low mean values and the high variances in the order parameters. When the radius exceeds a critical value, synchronization returns and persists (region I). When the radius deviates from that in the synchronization region, the wave patterns become disordered again. This situation lasts until the target radius reaches that for a lag synchronization region (region II) characterized by the mean value of $1/3$ in the order parameters with low variances. The lag synchronization region is relatively wide. For example, even when the target radius reaches $1/3$ of the half length of the square lattice, lag synchronization still occurs.

We are thus led to explore the dependence of the number of rings on the radius of the migration target for fixed values of intra- and inter-patch migration parameters. As shown in Fig. 6(b), there is apparently a correlation between the synchronization behavior and the number of rings. In particular, in the synchronization region, the number of rings is in the range between 3 and 6, while for lag synchronization the number is less than 3. Disorder arises when the number of rings in the target waves is more than 6.

IV. PHYSICAL THEORY

A. Number of rings associated with synchronization

To gain theoretical insights into pattern synchronization, we study the number of rings n_r associated with the target waves when synchronization occurs. Without loss of generality, we consider two patches A and B, as shown in Fig. 7. In each patch, the central species a is surrounded by b and b is surrounded by c. The average length L_r of an arbitrary species in A is

$$L_r = \mathbb{T} V = \frac{T_m V}{\langle \rho_B(c) \rangle - \langle \rho_B(b) \rangle}, \tag{6}$$

where V is the front propagation velocity of target waves and $\mathbb{T}$ is the time interval between two successful inter-patch migrations between two patches. Note that, only when species c moves to the migration target can a new ring be generated. Because, at each time step, the individual that executes actual migration is random, the time interval $\mathbb{T}$ for patch A is determined by the average species densities $\langle \rho_B(c) \rangle$ and $\langle \rho_B(b) \rangle$ in patch B from which individuals migrate, and vice versa. Given the lengths of the rings, n_r is given by $n_r = L/(\sqrt{2} L_r)$.

Since the front propagation velocity V does not depend on the inter-patch migration parameter T_m, it can be obtained by

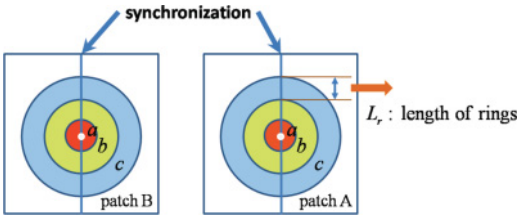

FIG. 7. (Color online) Schematic patterns for two patches in synchronization, where L_r defines the average length of rings.

casting the cyclically competing game in the framework of the complex Ginzburg-Landau equation (CGLE) [20]:

$$\partial_t z(\mathbf{r},t) = M\Delta z(\mathbf{r},t) + (c_1 - i\omega)z(\mathbf{r},t) - c_2(1 - ic_3)z(\mathbf{r},t)|z(\mathbf{r},t)|^2, \quad (7)$$

which is obtained by incorporating spatial diffusion terms into the rate equations. The CGLE describes the dynamical behavior of spatial patterns in a single patch in the absence of inter-patch migration. The spreading velocity of the propagating wave fronts can be determined by linearizing the CGLE around the unstable point $z = 0$ [37]:

$$\partial_t z(\mathbf{r},t) = M\Delta z(\mathbf{r},t) + (c_1 - i\omega)z(\mathbf{r},t) + o(z^2). \quad (8)$$

Performing the Fourier transform

$$\tilde{z}(\mathbf{k},\Omega) = \int_{-\infty}^{\infty} d\mathbf{r}\, dt\; z(\mathbf{r},t)\, e^{i\mathbf{k}\cdot\mathbf{r}+i\Omega t}$$

and substituting the inverted transform

$$z(\mathbf{r},t) = \int_{-\infty}^{\infty} d\mathbf{k}\, d\Omega\; \tilde{z}(\mathbf{k},\Omega)\, e^{-i\mathbf{k}\cdot\mathbf{r}-i\Omega t} \quad (9)$$

into the linearized CGLE, we obtain, for the left-hand side,

$$\partial_t z(\mathbf{r},t) = -i\Omega z(\mathbf{r},t). \quad (10)$$

The right-hand side of the CGLE is equal to

$$M\Delta z(\mathbf{r},t) + (c_1 - i\omega)z(\mathbf{r},t) = (-Mk^2 + c_1 - i\omega)z(\mathbf{r},t). \quad (11)$$

Equating the two sides, we obtain

$$\Omega(k) = \omega + i(c_1 - Mk^2). \quad (12)$$

The spreading velocity can be obtained by applying the saddle-point approximation (also known as the stationary phase or steepest descent approximation) [38]. In particular, for a saddle point k_*, we have

$$V \equiv \left.\frac{d\Omega(k)}{dk}\right|_{k_*} = \frac{\mathrm{Im}\,\Omega(k_*)}{\mathrm{Im}\,k_*}. \quad (13)$$

The solution to the saddle point k_* is found to be $k_* = i\sqrt{c_1/M}$. Thus, the spreading velocity is obtained as

$$V = 2\sqrt{c_1 M}, \quad (14)$$

where the coefficient c_1 is

$$c_1 = \frac{u\sigma}{2(3u+\sigma)}. \quad (15)$$

Due to pattern synchronization, the densities of species in patch A and patch B are identical:

$$\rho_A(b) = \rho_B(b) \quad \text{and} \quad \rho_A(c) = \rho_B(c). \quad (16)$$

We can then estimate the densities of species b and c in patch A during the propagation of the central ring occupied by a from zero to length L_r. The average density of c is

$$\langle\rho_A(c)\rangle = \int_{L_r}^{2L_r} \frac{\pi(x+L_r)^2 - \pi x^2}{L^2}\frac{1}{L_r}dx = \frac{4\pi L_r^2}{L^2}. \quad (17)$$

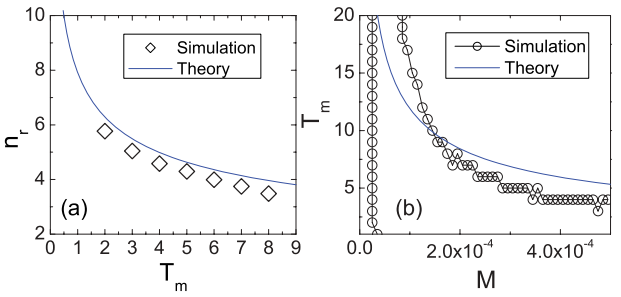

FIG. 8. (Color online) For a three-patch ecosystem, (a) the dependence of the number of rings on T_m in the synchronization regime for $M = 10^{-5}$ and (b) simulation and theoretical boundary between the target-wave and extinction regions in the parameter space. The curve in (a) is the theoretical results from Eq. (19) and the curve in (b) represents the estimate from Eq. (24).

Analogously, the outer boundary of species b to the center ranges from 0 to L_r, yielding

$$\langle\rho_A(b)\rangle = \int_0^{L_r} \frac{\pi(x+L_r)^2 - \pi x^2}{L^2}\frac{1}{L_r}dx = \frac{2\pi L_r^2}{L^2}. \quad (18)$$

Inserting $\langle\rho_A(c)\rangle$ and $\langle\rho_A(b)\rangle$ into Eq. (6) yields

$$n_r = \frac{L}{\sqrt{2}L_r} = \left(\frac{2T_m}{\pi L}\sqrt{\frac{u\sigma}{3u+\sigma}M}\right)^{-1/3}. \quad (19)$$

The analytical result agrees reasonably well with numerical simulations, as shown in Fig. 8(a).

B. Boundary between coexistence and extinction regions

The number of rings associated with a target-wave pattern turns out to be a useful indicator to understand the co-evolutionary spatiotemporal dynamics. For example, based on this number, we can estimate the boundary between the target-wave and extinction regions in the parameter space [Fig. 8(b)]. To demonstrate this, we consider a three-patch system. Without loss of generality, we can express the ring length in patch A as

$$L_r^A = \frac{T_m}{\frac{1}{2}[\langle\rho_B(c)+\rho_C(c)\rangle - \langle\rho_B(b)+\rho_C(b)\rangle]}V. \quad (20)$$

In the lag-synchronization state, we have $\langle\rho_B(c)+\rho_C(c)\rangle = 1$ and $\langle\rho_B(b)+\rho_C(b)\rangle = \langle\rho_B(b)\rangle$ (Fig. 9). For the extinction state, the length of the a ring in patch A satisfies the condition

$$L_r^A(a) > \frac{\sqrt{2}L}{4} \quad (21)$$

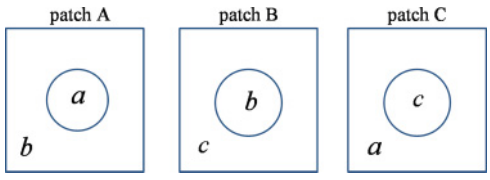

FIG. 9. (Color online) For a three-patch ecosystem, schematic illustration of patterns associated with the extinction state. In this route, there is still lag synchronization.

when a reaches the corners of the lattices. During this process, the quantity $\langle \rho_B(b) \rangle$ can be approximately calculated by

$$\langle \rho_B(b) \rangle \approx \int_0^{\sqrt{2}/2} \frac{\pi x^2}{L^2} \frac{1}{\frac{\sqrt{2}}{2}L} dx. \quad (22)$$

The parameter boundary between the target-wave and extinction regions can then be obtained by inserting Eq. (22) into Eq. (20) and setting $L_r^A(a) = \sqrt{2}L/4$:

$$\frac{\sqrt{2}L}{4} = \frac{T_m}{\frac{1}{2}(1 - \langle \rho_{0B}(b) \rangle)} 2\sqrt{\frac{u\sigma}{2(3u+\sigma)}} M, \quad (23)$$

which yields

$$T_m \approx \frac{1}{4}\left(1 - \frac{\pi}{6}\right) \frac{1}{\sqrt{M}}, \quad (24)$$

for $u = \sigma = 1$ and $L = 1$. This theoretical estimate of the boundary agrees reasonably well with that from direct stochastic simulations, as shown in Fig. 8(b).

V. OUTBREAK OF BIODIVERSITY AND COEXISTENCE OF DIFFERENT WAVE PATTERNS

A. Outbreak of biodiversity through rare and random mutations

An interesting issue is whether the combination of two types of migrations can induce a *spontaneous* outbreak of biodiversity from rare mutations in a single species world. To address this issue, we consider as an illustrative example a two-patch ecosystem and assume initially identical single species in both patches. We randomly reset the state of each individual with a small probability p to mimic the effect of random mutations that introduce two additional species in each patch. The three species then interact with each other cyclically, with migration occurring at all time. We then examine the spatial patterns and the lowest density $\rho_{\min}$ of species in each patch, a near-zero value of which would indicate extinction. As shown in Fig. 10, after a relatively long transient time, a sudden change from zero in $\rho_{\min}$ occurs, signifying coexistence. Accompanying this are target-wave patterns in both patches, ensuring persistence of all three species. This outbreak of biodiversity is triggered by the occasional appearance of new species in a patch as the result of mutation. Once there are three species in a patch, with nonzero probability, inter-patch migration can induce target waves which, in turn, warrant coexistence of all three species. In contrast, without inter-patch migration (effectively a single-patch environment), even though three species can occasionally appear simultaneously, the large differences among their densities will lead quickly to a predominant species, excluding the other two species, as represented by the small fluctuations of $\rho_{\min}$ about zero. Species coexistence can hardly be sustained without inter-patch migration even in the presence of random mutations.

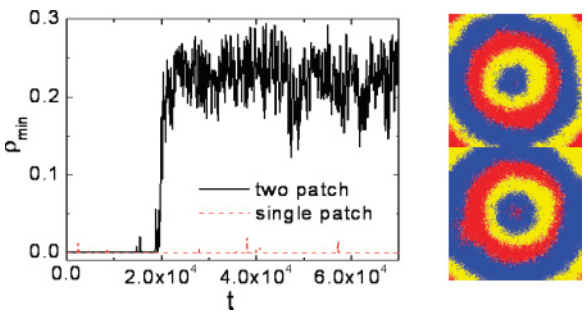

FIG. 10. (Color online) In a two-patch system, outbreak of biodiversity from random, rare mutations in a single species world for $M = 0.7 \times 10^{-4}$ and $T_m = 2$. Each lattice size is 200×200 with a central target region, and the mutation probability for each individual is 10^{-7} at each time step. The quantity $\rho_{\min}$ is defined as the density of the least frequent species in a patch, averaged over the two patches. Synchronized target waves are associated with the outbreak of biodiversity.

B. Coexistence of different waves and multitarget waves

We have observed the coexistence of target waves and spiral waves in different patches, which can occur regardless of the initial distributions of the populations. The coexistence is stable in the sense that the patterns are formed rapidly and each wave type cannot assimilate the other, as exemplified in Fig. 11. For the two-patch case, there is a spiral-wave basin in the phase space if the initial densities of the three species are close to each other. The coexistence of spiral and target waves occurs near the boundary of the spiral-wave basin. For the four-patch case in Fig. 11, spiral waves can be formed in the initially empty patch but never in other patches that are initially occupied by species. For the empty patch (patch D), due to the inter-patch migrations from other three patches, three species can be mixed around the migration target. There is thus a finite probability to form spiral waves centered at the target, as shown in Fig. 11. However, due to the randomness in the inter-patch migration, around the target point in patch D, the density differences among the three species can lead to a predominant species before the occurrence of spiral waves.

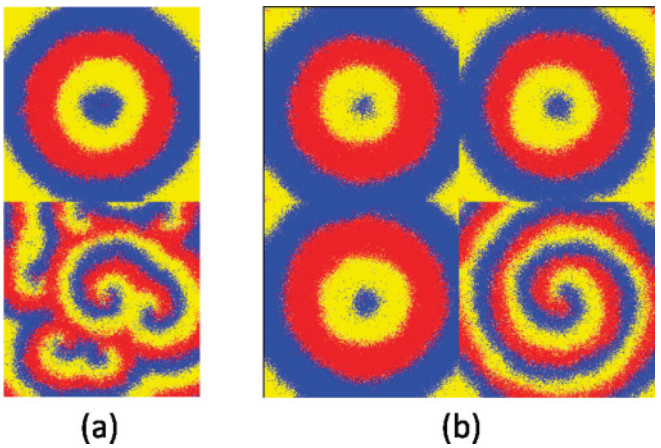

FIG. 11. (Color online) Coexistence of target and spiral waves for a two- and a four-patch system with central targets. For the two-patch system, species are mixed initially with the parameters $M = 0.6 \times 10^{-4}$ and $T_m = 1$. For the four-patch system, three species populate three patches, respectively, while the fourth patch is empty initially. The initial configuration, except the position of the target, is the same as that of Fig. 3. The parameters are $M = 1.2 \times 10^{-4}$ and $T_m = 1$. The lattice size of each patch is 300×300.

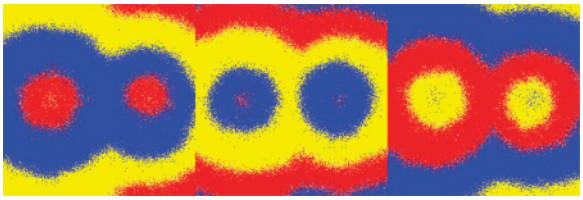

FIG. 12. (Color online) For a three-patch system, multitarget waves for $M = 0.8 \times 10^{-4}$ and $T_m = 1$. In each patch, there are two migration targets with the coordinates $(L/2,L/4)$ and $(L/2,3L/4)$, respectively. The lattice size is 300×300.

In this scenario, the predominant species will spread fast to the whole patch and the three species are unable to interact with each other sufficiently strongly at the migration target to generate spiral waves. We have observed that the spiral waves in patch D do not affect the synchronization of target waves among the other patches. It is noteworthy that an empty patch is a necessary condition for the birth of spiral waves in the case where other patches are of single species initially.

If there is more than one migration target region in a patch, multitarget waves can arise, as demonstrated in Fig. 12 for a three-patch system. There are two migration targets in each patch populated initially by a single species. We observe two coexisting target waves, each centered at a target region, forming an "eight" shape. Multiple target waves in a common patch are always synchronized. These behaviors have also been observed for three- and four-patch systems.

VI. BASINS OF SPECIES COEXISTENCE AND EXTINCTION

The basin of a final state is all initial configurations that lead to the state. In nonlinear dynamics, basins of attraction and the boundaries among them are a fundamental issue [39,40]. Consider again a two-patch ecosystem. A phase space can be defined by the initial densities of the three populations in both patches: $[\rho_A(a), \rho_A(b), \rho_A(c)]$ and $[\rho_B(a), \rho_B(b), \rho_B(c)]$. Since the phase space in terms of the population densities is six-dimensional, it is necessary to examine a reduced subspace for visualization and analysis. We choose the subspace defined by $\rho_A(a) = \rho_B(b)$, $\rho_A(b) = \rho_B(c)$, and $\rho_A(c) = \rho_B(a)$. In patch A (or B), the densities of the three species satisfy the constraint $\rho(a) + \rho(b) + \rho(c) = 1 - \rho_0$, where ρ_0 is the fraction of the empty sites. This conservation relation defines a triangular region in the plane, making the reduced phase space simplex S_2, where the coordinates of a point represent a group of three initial densities, and we can assign a color to a point in S_2 according to the resulting final state. Moreover, we also investigate the convergence time t_c, which provides additional information about the basin structures.

For the two-patch system with both intra- and inter-patch migration, there are six different evolutionarily steady states defining six distinct basins including three extinction and three coexistence basins distinguished by the three combinations of target and spiral waves. All three coexistence states are stable and determined by the initial configurations for fixed M and T_m. It can be argued that the state where two patches are occupied by two different species, respectively, is unstable, and identical single species in two patches is the exclusive extinction state, as follows. Without loss of generality, suppose that patches A and B are full of species a and b, respectively. Due to the cyclic competition and the presence of inter-patch migration, after individuals from a migrate from A to B, species b in patch B will begin to die and eventually become extinct, and patch B will be occupied by species a. Since there exist competitions between any two species, there can be only one species surviving in two patches as extinction occurs.

For comparison, we have also mapped out the basins for a single-patch system in the presence of intra-patch migration. Basins for one-patch and two-patch systems with different values of M and T_m are shown in Fig. 13. For the one-patch system (leftmost column), for small values of M, e.g., $M = 10^{-4}$, there is a spiral-wave basin at the center of the phase space S_2, surrounded by three entangled extinction basins. The areas of the spiral-wave and the extinction basins are determined by the mobility M. The spiral-wave basin is the sole coexistence basin, which arises when the initial densities of the three species are sufficiently close. As M is increased, the coexistence basin shrinks, accompanied by the expansion of the three extinction basins, which is consistent with the previous results that strong local mobility hinders coexistence [18–21]. When M exceeds a critical value 4.5×10^{-4}, the coexistence basin vanishes and biodiversity is lost.

In addition to basins characterized by final steady states, we also exploit the extinction time t_c to describe the basins of single patch, as shown in the bottom panels. We see that in the coexistence basin, $t_c \to \infty$ and $1/t_c \to 0$. In the vicinity of the boundary of two extinction basins, $1/t_c$ dramatically changes in two basins, and in each extinction basin, $1/t_c$ tends to decrease when rotating toward the center. The quantity $1/t_c$ thus provides further information about the dynamics inside basins in addition to the description of final stable states.

For the two-patch system (the second through fourth columns), the basins are characteristically changed as compared with the one-patch case. For example, for $M = 10^{-4}$, when the frequency of inter-patch migration is high, e.g., $T_m = 1$, a vast area of double target-wave basin emerges in the phase space, whereas extinction basins can hardly be observed. At the center, the double spiral-wave basin is preserved, surrounded by the one spiral- and one target-wave basin. We see that coexistence is enhanced considerably by inter-patch migration, as characterized by the presence of a vast area of coexistence basins, regardless of the heterogeneity in the initial population densities. This is a surprising feature as population heterogeneity has been thought to be disadvantageous for species coexistence. When the period of inter-patch migration is increased, e.g., $T_m = 15$, small areas of extinction basins inside the vast target-wave basin arise with a rotational symmetry. We can expect that, when T_m becomes increasingly large, the basin structure in the two-patch system tends to the structures from the one-patch system. For large values of M, e.g., $M = 3.0 \times 10^{-4}$, for the single patch, the coexistence basin nearly vanishes, while for the two-patch system with $T_m = 1$, a double target-wave basin arises in the central area and along the boundary among different extinction basins. For low frequency of inter-patch migration, e.g., $T_m = 15$, the double target-wave basin only exists at the center. Although the basin structure can be dramatically changed with respect

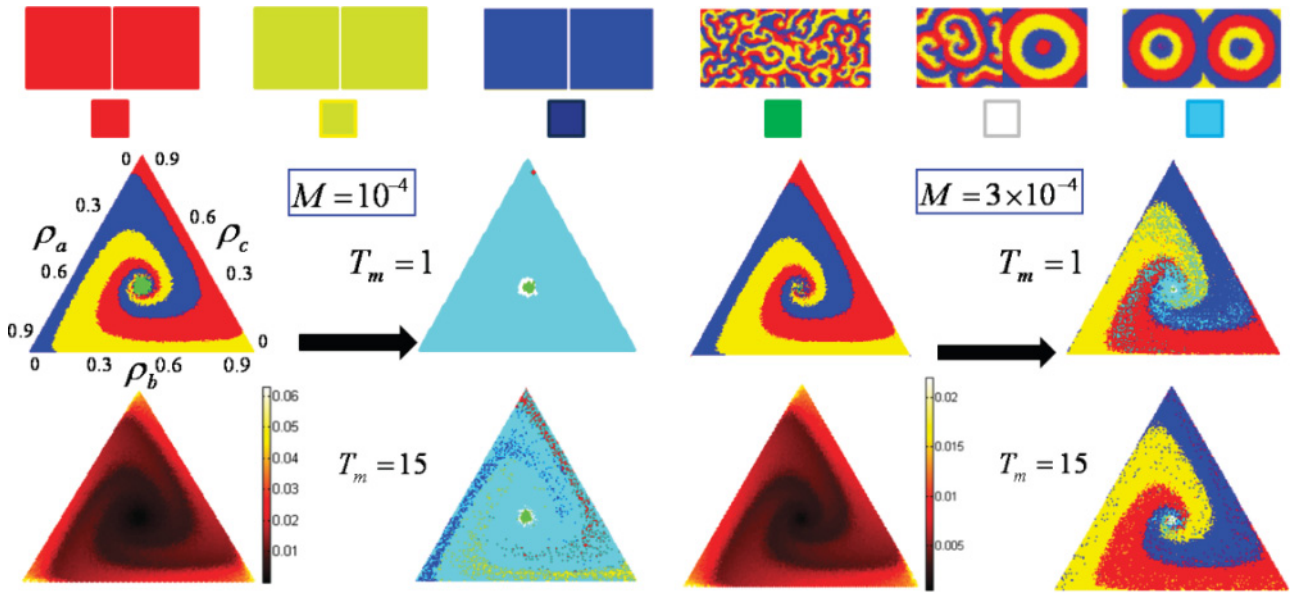

FIG. 13. (Color online) For a single-patch and a two-patch system, basins of extinction, target waves, and spiral waves, where the size of each patch is 200 × 200. There are six different evolutionary steady states: three extinction states, a double spiral-wave state, one spiral- and one target-wave state, and a double target-wave state. They are distinguished by different colors. For the single patch (the leftmost column), all the basins exhibit a rotational symmetry around the center point ($M = 10^{-4}$). As M is increased, the area of the coexistence basin is reduced. The bottom panels for the single patch show the inverse $1/t_c$ of the convergence time t_c for different initial densities of species. For the two-patch system (the second through fourth columns), a vast area of target-wave basins can arise, promoting biodiversity. Note that the extinction basins appear clockwise compared to the basins in a single patch.

to the inter-patch migration, the rotational symmetry is always preserved.

VII. CONCLUSIONS AND DISCUSSIONS

Our results demonstrate that the interplay between intra- and inter-patch migrations in multipatch ecosystems under cyclic competition can lead to remarkable target-wave patterns originating from stochastic interactions. These self-organized waves can emerge either from mixed populations or from single species in an individual patch in the absence of external control. Target waves can form regardless of the area and the position of the migration target and the number of patches. Moreover, multitarget waves can be induced by multiple migration targets in a single patch, and target waves and spiral waves can coexist stably. Strikingly, for proper combination of intra- and inter-patch migration rates, synchronization and lag synchronization of target-wave patterns among different patches can occur, depending on the area of the migration target. Analytic insights into the synchronization dynamics have been obtained through the dependence of the number of rings associated with target waves on the migration parameters. Our computations have also revealed the phenomenon of outbreak of biodiversity from single species through rare mutations. The mapping of the basin structure in a proper phase space provides further support for the robustness of target waves in sustaining species coexistence, where both biodiversity and extinction basins typically exhibit rotational symmetry in the simplex S_2.

It is noteworthy that the synchronization phenomena resulting from stochastic interactions at the microscopic level can have important applications. For example, pattern synchronization stabilizes species persistence in a remarkable order, in contrast to viewing population synchronization as a cause of global population extinctions. Further, the lag synchronization enables possible prediction of the future spatiotemporal evolution of species based on current dynamical behavior in an arbitrary patch. In particular, due to the nature of lag synchronization, the spatiotemporal feature at the present in one patch will be experienced by others in a future time. This can be extremely useful for anticipating evolutionary dynamics in ecosystems and developing effective control strategy in advance to protect species diversity.

The outbreak of biodiversity via target-wave pattern from single species with rare mutations demonstrates the robustness of target waves in facilitating species coexistence. This phenomenon also provides a possible approach to the exploration of species in history. The combination of simple migration behaviors and natural selection, two typical mechanisms for self-organization, can successfully support species balances in nature.

Our results are also relevant to the origin of order [41], a significant issue in nature and society, which has been discovered in Boolean dynamics for modeling regulatory networks. There exist periodic attractors in the phase space that lead to a number of periodic dynamical behaviors. In our study, both spatial and temporal orders emerge from disordered states, even from single species in a noisy world, as the result of two types of migrations and stochastic interactions. When synchronization occurs, time evolutions of species densities become approximately periodic and, spatially, the target waves in different patches exhibit identical length of rings. Migrations over distant space provide an alternative route to the emergence of spatiotemporal order in addition to Boolean dynamics.

ACKNOWLEDGMENTS

This work was supported by AFOSR under Grant No. FA9550-10-1-0083, by NSF under Grants No. BECS-1023101 and No. CDI-1026710, by a seed grant from the National Academies Keck Futures Initiative (NAKFI) on Complex Systems, by BBSRC under Grants No. BB-F00513X and No. BB-G010722, and by the Scottish Northern Research Partnership.

[1] R. M. May, *Stability and Complexity in Model Ecosystems* (Princeton University Press, Princeton, NJ, 1973).
[2] D. Tilman and S. Pacala, in *Species Diversity in Ecological Communities*, edited by R. E. Ricklefs and D. Schluter (University of Chicago Press, Chicago, 1993), pp. 13–25.
[3] J. Hofbauer and K. Sigmund, *Evolutionary Games and Population Dynamics* (Cambridge University Press, Cambridge, England, 1998).
[4] J. Maynard Smith, *Evolution and the Theory of Games* (Cambridge University Press, Cambridge, 1982).
[5] K. Sigmund, *Games of Life* (Oxford University Press, Oxford, 1993).
[6] A. M. Colman, *Game Theory and its Applications in the Social and Biological Sciences* (Butterworth-Heinemann, Oxford, 1995).
[7] M. A. Nowak, *Evolutionary Dynamics* (Belknap Press, Cambridge, MA, 2006).
[8] G. Szabó and G. Fath, Phys. Rep. **446**, 97 (2007).
[9] J. B. C. Jackson and L. Buss, Proc. Natl. Acad. Sci. USA **72**, 5160 (1975).
[10] C. E. Paquin and J. Adams, Nature (London) **306**, 368 (1983).
[11] B. Sinervo and C. M. Lively, Nature (London) **380**, 240 (1996).
[12] T. L. Czárán, R. F. Hoekstra, and L. Pagie, Proc. Natl. Acad. Sci. USA **99**, 786 (2002).
[13] R. M. May, Science **186**, 645 (1974).
[14] R. M. May and W. J. Leonard, SIAM J Appl. Math. **29**, 243 (1975).
[15] A. Traulsen, J. C. Claussen, and C. Hauert, Phys. Rev. Lett. **95**, 238701 (2005).
[16] J. C. Claussen and A. Traulsen, Phys. Rev. Lett. **100**, 058104 (2008).
[17] L. Pagie and P. Hogeweg, J. Theor. Biol. **196**, 251 (1999).
[18] G. Szabó, J. Phys. A **38**, 6689 (2005).
[19] G. Szabó, A. Szolnoki, and G. A. Sznaider, Phys. Rev. E **76**, 051921 (2007).
[20] T. Reichenbach, M. Mobilia, and E. Frey, Nature (London) **448**, 1046 (2007); Phys. Rev. Lett. **99**, 238105 (2007); J. Theor. Biol. **254**, 368 (2008).
[21] D. Helbing and W. Yu, Proc. Natl. Acad. Sci. USA **106**, 3680 (2009).
[22] W.-X. Wang, Y.-C. Lai, and C. Grebogi, Phys. Rev. E **81**, 046113 (2010).
[23] R. Yang, W.-X. Wang, Y.-C. Lai, and C. Grebogi, Chaos **20**, 023113 (2010).
[24] M. C. Gonzáles, C. A. Hidalgo, and A. L. Barabási, Nature (London) **453**, 779 (2008).
[25] S. A. Levin, Am. Nat. **108**, 207 (1974).
[26] P. M. Hassell, H. N. Comins, and R. M. May, Nature (London) **353**, 255 (1991).
[27] R. D. Holt, J. Grover, and D. Tilman, Am. Nat. **144**, 741 (1994).
[28] B. Blasius, A. Huppert, and L. Stone, Nature (London) **399**, 354 (1999).
[29] C. L. Lehman and D. Tilman, in *Spatial Ecology: The Role of Space in Population Dynamics and Interspecific Interactions*, edited by D. Tilman and P. Kareiva (Princeton University Press, Princeton, NJ, 1997), pp. 185–203.
[30] Y.-C. Lai and Y.-R. Liu, Phys. Rev. Lett. **94**, 038102 (2005).
[31] Target wave patterns were previously found in excitable systems. See, for example, E. Pálsson and E. C. Cox, Proc. Natl. Acad. Sci. USA **93**, 1151 (1996); K. J. Lee, Phys. Rev. Lett. **79**, 2907 (1997).
[32] A. N. Zaikin and A. M. Zhabotinsky, Nature (London) **225**, 535 (1970).
[33] K. J. Lee, E. C. Cox, and R. E. Goldstein, Phys. Rev. Lett. **76**, 1174 (1996).
[34] K. J. Lee, Phys. Rev. Lett. **79**, 2907 (1997).
[35] T. J. Lewis and J. Rinzel, Net. Comput. Neural Syst. **11**, 299 (2000).
[36] G. Szabó, A. Szolnoki, and R. Izsák, J. Phys. A **37**, 2599 (2004); A. Szolnoki and G. Szabó, Phys. Rev. E **70**, 037102 (2004); C.-Y. Ying, D.-Y. Hua, and L.-Y. Wang, J. Phys. A: Math. Theor. **40**, 4477 (2007).
[37] M. C. Cross and P. C. Hohenberg, Rev. Mod. Phys. **65**, 851 (1993).
[38] W. van Saarloos, Phys. Rep. **386**, 29 (2003).
[39] S. W. McDonald, C. Grebogi, E. Ott, and J. A. Yorke, Physica D **17**, 125 (1985).
[40] H. Shi, W.-X. Wang, R. Yang, and Y.-C. Lai, Phys. Rev. E **81**, 030901(R) (2010).
[41] S. A. Kauffman, *Origins of Order* (Oxford University Press, Oxford, 1993).